Hindawi
International Transactions on Electrical Energy Systems
Volume 2022, Article ID 2915910, 21 pages
https://doi.org/10.1155/2022/2915910

Research Article

Optimized Convolutional Neural Network-Based Capacity Expansion Framework for Electric Vehicle Charging Station

A. S. Monikandan,[1] **C. Chellaswamy**,[2] **T. S. Geetha**,[3] **and S. S. Sivaraju**[4]

[1]*Department of Electrical and Electronics Engineering, Arunachala College of Engineering for Women, Nagercoil, India*
[2]*Department of Electronics and Communication Engineering, SRM TRP Engineering College, Tiruchirappalli, India*
[3]*Department of Electronics and Communication Engineering, Sriram Engineering College, Chennai, India*
[4]*Department of Electrical and Electronics Engineering, RVS College of Engineering and Technology, Coimbatore 641402, India*

Correspondence should be addressed to C. Chellaswamy; chellaswamyc@lords.ac.in

Received 2 October 2021; Revised 25 December 2021; Accepted 17 January 2022; Published 24 March 2022

Academic Editor: Tianqi Hong

The usage rate of electric vehicles (EVs) is gradually increasing. Recharging of EVs should be carried out repeatedly over time, and the energy needed for this is high and increasing. With the present infrastructure, we cannot supply the required energy, and therefore, we need to implement a model that expands the power grid to satisfy our energy requirements. This paper proposes a convolutional neural network-based dynamic capacity expansion (CNN-DCE) for EV charging. Flower pollination optimization algorithm (FPOA) was used to improve the hyperparameters of CNN during training. The main aim is to reduce the cost of installing additional capacity resources and to reduce the operational cost. To cope with the load growth, different capacity resources are installed at different years of the planning boundary. Five statistical indices, such as mean squared error, mean absolute error, correlation coefficient, and scatter index, are used to evaluate the performance of CNN. The capacity expansion plan in the microgrid is achieved by expanding the energy of battery energy storage systems, microturbines, and solar and wind energy systems. The queuing delay for the EVs waiting in a queue for recharging has been considered. The performance of the proposed CNN-DCE is studied and compared with three other state-of-the-art methods. The results show that the resources reduce the planning cost to 26% for the short-term planning horizon, the long-term plan has 150% of the expansion, and the wind energy system covers 48% of the expansion cost.

1. Introduction

Energy-efficient and cleaner transportation systems can be obtained by increasing the use of electric vehicles (EVs). There are many reasons for an increase in the adoption rate of EVs. Firstly, due to the advancement in battery storage, Tesla has designed a model to travel around 300 miles with a single charge [1]. Also, the US government has introduced many schemes to increase the sale of EVs. Grand Challenge of EV was initiated by US Energy Secretary Ernest Moniz in 2014, and $50 million was allocated for research to produce cheaper and more convenient EVs by 2022 [2]. With the increase in the use of EVs, harmful and rare fossil fuel usage is reduced. When the charge of the EVs depletes, recharging is done at the charging station (CS), and as there is an increase in uptake of EVs, the CS needs to be expanded [3]. Sufficient energy from the power grid is needed to recharge the batteries. Most power grids do not supply enough energy to meet the demand arising from CS. Thus, expansion of power is needed [4]. A survey from Washington State's Transport Department shows 228,725 kWh of energy was needed to charge cars between 2012 and 2015, which is equal to the displacement of 22,397 gallons of gas [5]. Figure 1 shows the monthly usage of the newly opened station in 2012, which, by December 2015, was 25,888 times higher. It is anticipated that, by 2029, the load from EVs will reach 108 MW in Washington; therefore, some measures have to be taken to meet the additional requirement for power [6].

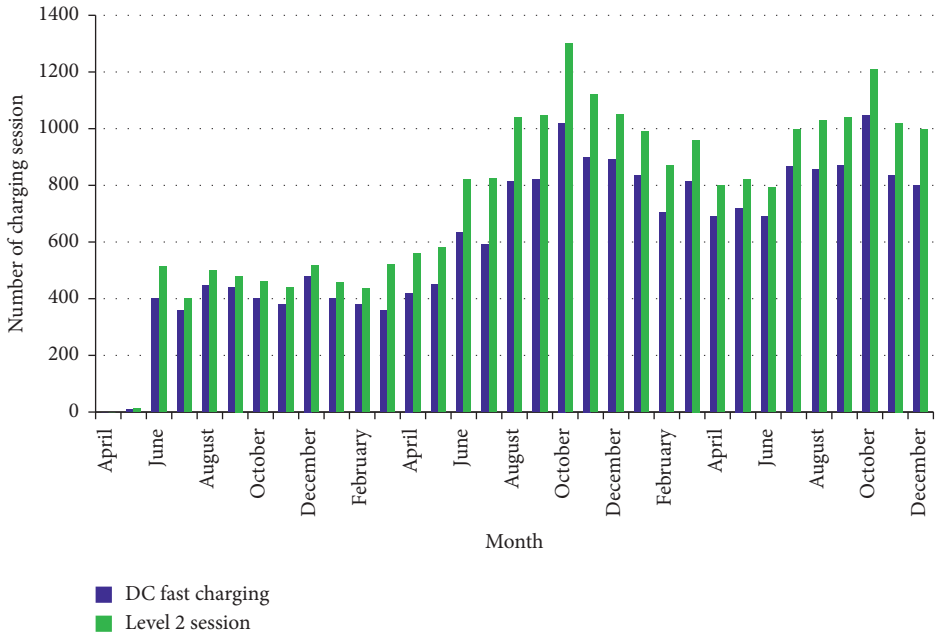

Figure 1: Monthly charging session of a station from 2012 to 2015.

In recent years, microgrids have been developed as an important part of electrical grids. These microgrids can also be used for expansion planning [7, 8, 9]. The capacity of lines and energy resources are less for microgrids when compared to electric power systems. Other energy resources, namely, wind, gas turbine, battery energy storage systems (BESS), and solar and diesel power generation, can be integrated with a microgrid [10, 11]. In the upcoming years, the load demand can be met by expanding the available energy resources. We can also expand the capacity of the connected line between the upstream network and the microgrid [12]. In microgrids, BESS plays a key role, and many technical and economic advantages of applying hybrid energy storage systems in the microgrids are discussed by Tang et al. [13]. A short-term hybrid, such as battery-flywheel hybrid, and long-term hybrids, such as compressed air-super capacitor combination, are available in hybrid storage. In the future, unbalanced and nonlinear loads can be used for the application of hybrid energy storage systems [14, 15, 16]. A bidirectional electric vehicle charging station with a multistep current control strategy is introduced by Balasundar et al. The power flow from vehicle-grid and grid-vehicle is facilitated by the bidirectional converters [17]. A robust location-based electric EV charging station combined with grid and the road network is suggested by Li et al. The capacity of the storage system, solar PV system, and wind energy system is determined using fitness value between the charging demand curve and the uncertain output curve of renewable energy [18].

Various problems related to the location of electric vehicle charging stations (EVCS) have been discussed by many researchers. Pan et al. propose a clustering method to meet the demand for EVs needing to charge in urban areas and a plan to locate the battery-operated EVCS [19]. Power companies in different geographic regions decide on a power grid's expansion each year; however, since the demand for EVs charging in a location depends on an uncertain adoption rate, each company must decide to expand the power grid to support the installation of CS over a timeframe [20]. Chen and Kockelman determine the location of EVCS in parking locations by regressively analyzing parking survey data [21]. The maximal covering model is used by Frade et al. to find the location of EVCS within Lisbon and Portugal [22]. Another method, Flow Refueling Location Model (FRLM), is used to estimate the coverage of many EVCS along with round trips [23]. Bouche et al. find the energy consumed by the EVs using origin-destination (OD) data based on a realistic trip, and an integer programming model is formulated to find the optimal EVCS location [24]. Chung and Kwon proposed a multitime period planning model to determine the location of the EVCS when FRLM is used as a foundation. To solve the multitime period optimization model, forward and backward myopic methods are used [25].

In addition to this, more research has been conducted to develop a random model to determine the location of EVCS. A two-stage random programme was developed by Pan et al. to find the location of EVCS before realizing the battery demands, loads, and renewable power source generation capacity [26]. A three-step method that combines simulation and optimization is used to find the location of EVCS and the level of charging to be installed at each CS [27]. A multitime period linear mixed-integer programming model is used to find an optimal control strategy for an EVCS that has power storage, renewable energy sources, and integrated EVs. Further, a random chance-constrained programming model is proposed by them, which manages demand and power generation, connection and disconnection times, and

state of EV charge [28]. Using the limited amount of information about EV's adoption rate, Mak et al. proposed an optimization model to build the infrastructure for EV swapping stations [29]. Surendar and Bijwe suggested a day-ahead optimal power flow control, including renewable energy resources [30]. A two-stage station location model using stochastic refueling is proposed by Hosseini and MirHassani, which is based on a finite number of situations that have traffic flow uncertainty [31]. Zhu et al. proposed an optimized framework that provides multiple EVCS, so a number of cars can charge simultaneously. The key idea is that using this optimal control method, charging costs can be reduced, and EVs can be charged with the optimal rate [32]. A stochastic model is proposed to operate EVCS effectively under stochastic demand using an energy storage device [33]. The optimization problem is solved by a two-step algorithm in which the problem size is reduced in the first step by solving the original model, and the location of the EVCS is determined by using a greedy algorithm in the second step [34]. The computational cost is higher. As a result, the proposed method incorporates FPOA for computational efficiency.

In some studies, battery swapping was considered instead of charging the batteries of the vehicle. The discharged batteries of the EV are substituted with the fully charged batteries present in the charging station [35,36]. The EV battery packs are charged along with the roadside wireless charging system while running [37]. The unknown service time of a recharging station must be considered, and the waiting time of EV increases if it has a limited number of chargers. Froger et al. have studied related problems in which the EV is waiting due to the chargers being busy [38]. In this problem, the chargers of the recharging station depend on the charging decision and the routing. On the other hand, the proposed method setting the queue lengths is autonomous for these features. The waiting times at the alternative fuel filling station have been studied by Bruglieri et al. [39]. The alternate fuel vehicles are routed in such a way that the times of refueling do not overlap with other EVs. So in this study, deterministic queuing is included for estimating the waiting time of EVs.

Machine learning is one of the most interesting computational methods for learning from interaction. It is a goal-oriented learning approach interacting with an uncertain environment [40]. Convolutional neural networks (CNNs) are computational models inspired by biological nervous systems (not identical). CNN can solve complex and nonlinear problems with higher accuracy [41]. In this paper, a CNN-based dynamic capacity expansion plan (CNN-DCE) is proposed for EVCS, including microgrid and various energy resources. Recently, optimization algorithms have been used in a neural network for increasing the accuracy. In the pioneering work [42], a comparative analysis among FPOA, particle swarm optimization (PSO) algorithm, and genetic algorithm (GA) shows that FPOA utilized few control parameters with the promising capability in terms of convergence speed and accuracy. Further, FPOA is used in various real-world applications such as visual shape matching [43], machining process [44], and scheduling [45,46]. These distinct characteristics of FPOA motivate the authors to integrate it into the capacity expansion problem. In this study, the FPOA was used to optimize the hyperparameters of CNN for providing an optimal solution. The proposed FPOA optimized CNN-DCE was compared with three other state-of-the-art methods: PSO, fruit fly optimization (FFO) algorithm, and firefly optimization technique (FOT).

The main contribution of this study is as follows:

(i) CNN-DCE has been proposed to develop a machine learning-based capacity expansion for accurate and faster estimation

(ii) A comprehensive review among optimization techniques FPOA has been selected due to the utilization of a few control parameters applied to the convolutional neural network (CNN) for optimizing the hyperparameters of the CNN layer during training

(iii) The performance of the proposed CNN-DCE has been compared with other widely used algorithms, PSO, FFO, and FOT

(iv) The performance of the proposed method has been assessed using four different statistical indices

The remaining part of this paper has been organized as follows: Section 2 describes the proposed capacity expansion plan and the workflow. Section 3 provides the mathematical model with different constraints. Section 4 presents the training and testing experiments. Result and discussion are provided in Section 5. Finally, the conclusion is given in Section 6.

2. Proposed System

The electricity used in the microgrid may be generated by diesel, gas turbines, or renewable energies. For a smoother operation of EVs, a microgrid uses energy storage devices to provide electricity to the electric and thermal loads [47]. A microgrid is a separate entity and continues its operation even if an upstream grid is not functioning due to a blackout. A microgrid connected to the upstream grid and the EVCS, including various resources, is shown in Figure 2. Resources like solar energy and wind energy are connected as renewable sources, and micro gas turbines are connected as nonrenewable sources to the microgrid. Whenever there is an unavailability of renewable energy, nonrenewable sources are used. When the microgrids are connected to the CS, the plugged-in EVs can either send energy to the grid or charge it by regulating its charging rate and time [48,49]. The connections from the microgrid to the generating resources and load are unidirectional, and connections to the EVCS and energy storage device are bidirectional. The microgrid operation is optimized by the control centre by taking economic conditions, autonomous operation, technical restrictions, and grid-tied operation into account.

2.1. Model of Capacity Expansion Plan. A microgrid uses the utility grid and capacity resources to supply the demand of

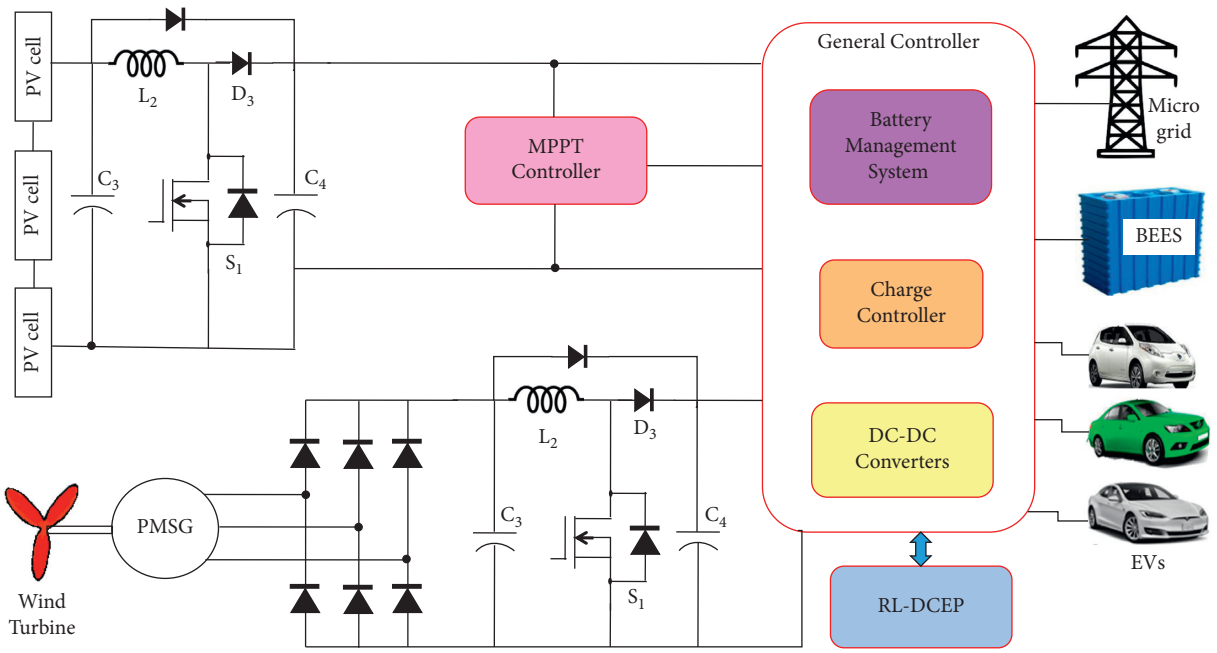

Figure 2: Microgrid connected to EVCS including various sources.

the load. With this capacity, a microgrid cannot meet the demand as the load demand increases in upcoming years, so capacity resources must be expanded. A plan to expand the capacity resources is performed on the microgrid to obtain the size, operation, time, and technology of the new resources that could be mounted onto a microgrid. This expansion plan will meet the increase in demand by considering technical and economic aspects. In this paper, to obtain the capacity expansion model, wind, solar, energy storage devices and micro gas turbines are used as resources. Annual growth of the load is used to estimate the expansion of capacity resources to meet the demand.

2.2. Short-Term and Long-Term Plans. A flowchart to describe the model is shown in Figure 3. The expansion model consists of two plans in which the long-term plan uses installation optimization for the microgrid's new resources, and the short-term programme is used to determine the exact operation method for dispatched resources. A mixed linear integer programme is obtained by combining the two plans, and it reduces the overall operational, maintenance, and investment costs. A long-term plan determines the investment cost of installing new capacity resources. The peak demand for the load is met by using existing and installed capacity resources.

It must be scheduled properly, so further installation of resources can be avoided. For example, in order to meet the peak demand of the load, energy storage devices can be released to avoid any installation of new resources. A short-term plan helps to use the resources efficiently, so the long-term plan of installing new resources can be avoided to result in lower investment costs. Thus, the long-term plan is used to install energy resources, and the short-term plan efficiently uses these resources so the long-term plan can install

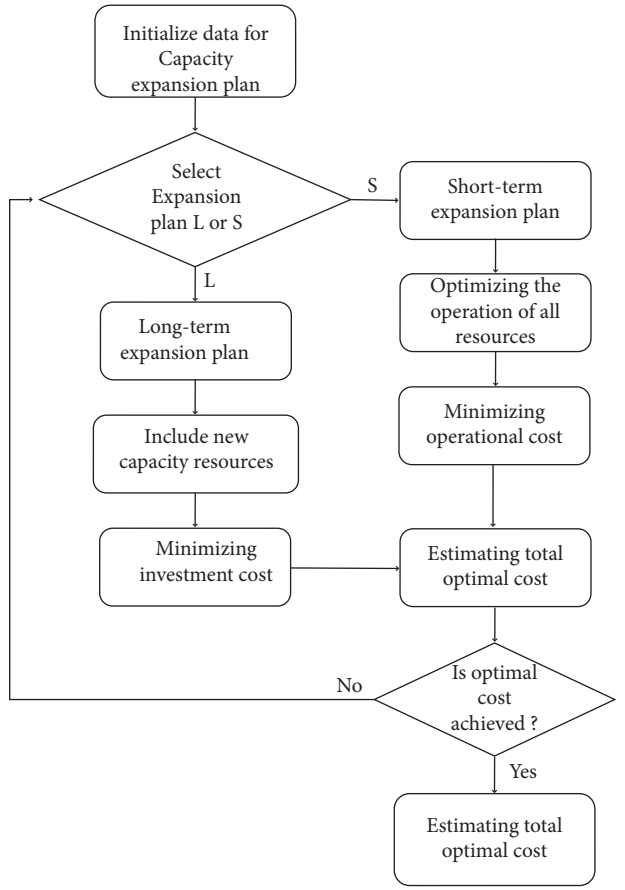

Figure 3: Flowchart of the proposed capacity expansion model.

such resources with smaller capacities. Resources are efficiently used by finding the optimal operation of energy storage devices, micro gas turbines, and EVCS. For example,

a short-term plan is used to regulate the energy sent by EVCS to the microgrid, its charging rate, and time, reducing the long-term plan of installing additional resources.

2.3. Workflow. In this study, CNN was utilized to increase detection accuracy. It is a type of deep learning model that easily adds more layers. CNN can process the raw input data without preprocessing. Initially, the CNN architecture extracts the features of the input data using several layers, including a convolutional layer (CL) and after that a maximum pooling layer (MPL). To classify the input features, a fully connected layer (FCL) and a classification layer were used. The gradient descent training algorithm was used to tune the weights and biases composed by the CLs and FCLs. Various hyperparameters such as learning rate, momentum, regularization, validation frequency, and several epochs strongly reflected the performance of the training algorithm. In this study, FPOA was proposed to optimize these hyperparameters of CNN-delivered optimal solutions during training. The flow diagram of the proposed architecture for optimizing the hyperparameters of CNN using FPOA is shown in Figure 4.

2.3.1. Hyperparameter Optimization. In this study, the hyperparameters of CNN were optimized using FPOA. The selection of a number of samples per iteration in FPOA plays a vital role. It introduces false randomness during nonjudicious selection in a number of samples. It leads to premature convergence. By referring to the previous literature and conducting repeated simulations, CNN-DCE utilized 5 samples per iteration. In addition, parameters tuning is one of the significant factors that influence the rate of convergence. The computational burden gets increased if a higher number of parameters is tuned. Fortunately, FPOA has only two parameters (probability switch and scaling factor) for tuning. Therefore, FPOA is selected in this study. The speed of convergence and accuracy of CNN was determined by its hyperparameters. Based on the application, the hyperparameters of CNN should be selected. Various hyperparameters are mentioned in Section 2.3, in which the momentum controlled the weight update, learning rate controlled the speed of the gradient descent algorithm, several epochs determined the number of updates done by the learning algorithm according to the training dataset, and the regularization parameter resolved the overfitting problem present in the network. Hence, to achieve better performance of the network, it is necessary to optimize all these hyperparameters. The proposed FPOA optimized different hyperparameters of CNN during training given in Algorithm 1.

3. Problem Formulation

The charging station is integrated with energy sources and energy storage systems. Mathematical model of power generation and storage systems, various constraints, and the CNN is used for the capacity expansion problem. The operational, maintenance, and investment costs have been considered for all the energy sources with different capacities. The investment cost of the charging station is converted to a corresponding annual amount, and then the net value is performed. In this work, the salvage rate has not been considered, and a 10% discount rate has been considered.

3.1. Structure of CNN-DCE. The structure of the proposed CNN-DCE is shown in Figure 5. It consists of data acquisition, data modeling, and data analysis. The input data is processed by the data acquisition unit. Due to the occurrence of an error during data storage or a failure of the charger, data of the CS may be distorted. As a result, estimation of the power consumption model creates a serious problem. Hence, before modeling the electric power consumption using the raw data, it compares with the historical data and removes the errors that make it fit for the estimation model. The data modeling performs the model for estimating the power required charging each EV and the requirement for the expansion using the number of chargers in the charging station and charging times. It provides the relationship between different variables such as the charging power, the charging time, number of chargers in the charging station, predictor variables, weights for the predictor variables, and the error. The database is used to map the real-time data with location information; the proposed CNN-DCE monitors the charging station for managing the consumption control, flow control of EVs, and managing the load limit. The proposed CNN-DCE updates the information periodically, thereby monitoring the electric power consumption during a specific period for each charging station in real-time.

3.2. Mathematical Model. The investment and operational cost of the solar PV system, wind power system, microturbine, inverter, and ESS are modeled. The investment cost of the solar PV system (C_{cost}^{PV}) is expressed as

$$C_{cost}^{PV} = \sum_{y \in Y} \left(NI_{PV}^{y} \times P_{PV} \times R_{PV} \times N_{eq} \times N_{P1} \right), \tag{1}$$

where NI_{PV}^{y}, P_{PV}, and R_{PV} denote, respectively, the newly installed solar PV system each year, the rated power of the solar PV system, the price of the solar system. The equivalent annual cost $N_{eq} = D \times (1 + D)^{L} / (1 + D)^{L} - 1$, the net present value $N_{P1} = N_f / (1 + D)^{L}$, and D, L, and N_f are the discount rate, asset lifetime, and net cash flow, respectively. y is the index of years and Y is the set of years. The operational and maintenance cost of the solar PV system is expressed based on [48] as

$$C_{op}^{PV} = \sum_{y \in Y} \left(PV_{a}^{y} \times P_{PV} \times O_{PV} \times N_{P1} \times 365 \right), \tag{2}$$

where PV_{a}^{y} and O_{PV} are the available solar power in a year (%) and the operational cost of the PV system ($/year), respectively. The investment cost of the wind power system (C_{cost}^{WP}) is expressed as

$$C_{cost}^{WP} = \sum_{y \in Y} \left(NI_{WP}^{y} \times P_{WP} \times R_{WP} \times N_{eq} \times N_{P1} \right), \tag{3}$$

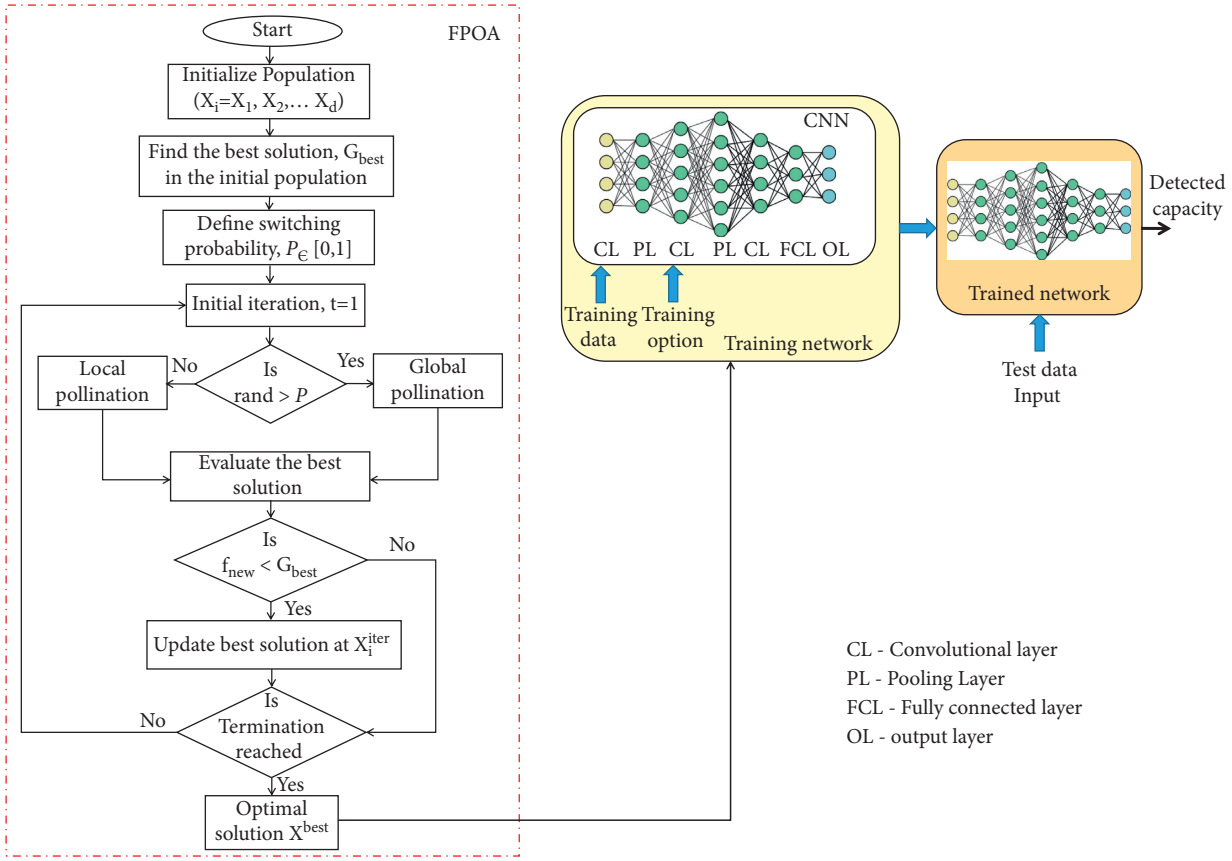

Figure 4: Flow diagram of FPOA optimized CNN for capacity expansion problem.

Take batch size: m, hyperparameters: P_1, P_2, P_3, and P_4, number of iterations: N, dimension: d, number of search agents: n, and evaluation function of hyperparameters: H_e.
Determine the objective function, $f(x_i)$, $X_i = (X_1, X_2, \ldots X_d)$
Define maximum iteration = max_iter; global best solution (G_{best})
Define iteration, $t = 1$; switch probability, p
Initialize the pollination of n flowers randomly,
Sample of batch of training data
while ($t <$ max_iter)
for $i = 1{:}n$
  If rand $> p$
    Draw a step vector L which obeys a Lévy distribution
    Perform a global search using $X_i^{t+1} = X_i^t + L(X_i^t - G_{best})$
  else
    Select a and b randomly among all the solutions
    Randomly choose β from a uniform distribution [0, 1].
    Do a local search using $X_i^{t+1} = X_i^t + \beta(X_a^t - X_b^t)$
  endif
    Evaluate new solutions (f_{new}) and update them if they are
    Better
    If f_{new} is better than G_{best}, update G_{best} and its fitness
end for
  Estimate the best solution
  (P_1, P_2, P_3, P_4) = hyperparameter evaluation function (f_h),
  $t - t + 1$
end while

Algorithm 1: FPOA optimization algorithm for updating the hyperparameters of CNN.

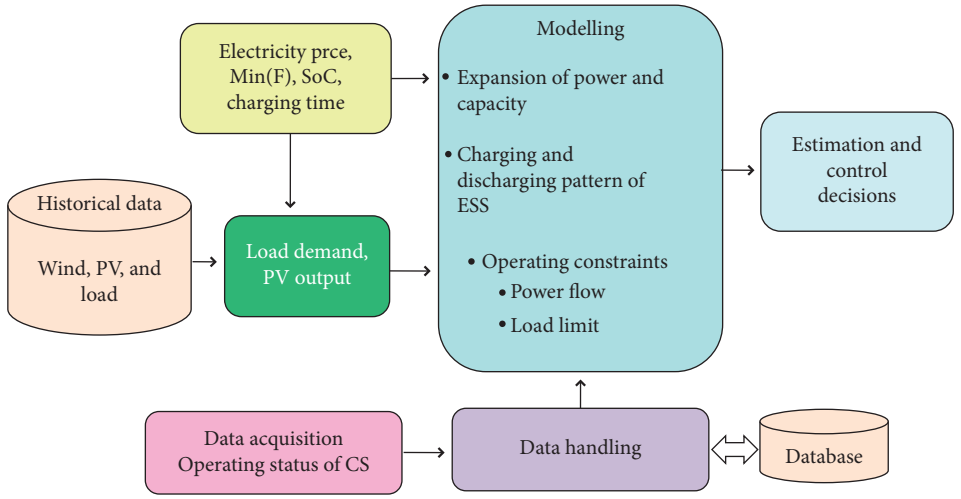

Figure 5: Structure of the proposed CNN-DCE.

where NI^{y}_{WP}, P_{WP}, and R_{WP} denote, respectively, the newly installed wind power each year (%), the rated power of wind system (kW), and the price of wind system ($/kW). The operational and maintenance cost of the wind power system (C^{WP}_{op}) is expressed based on [48] as

$$C^{WP}_{op} = \sum_{y\in Y}\left(WT^{y}_{a} \times P_{WP} \times O_{WP} \times N_{P1} \times 365\right), \tag{4}$$

where WT^{y}_{a} and O_{WP} denote, respectively, the available wind power each year (%) and wind system operational cost ($/kW). The investment cost of the microturbine (C^{MT}_{cost}) is expressed as

$$C^{MT}_{cost} = \sum_{y\in Y}\left(NI^{y}_{MT} \times P_{MT} \times R_{MT} \times N_{eq} \times N_{P1}\right), \tag{5}$$

where NI^{y}_{MT}, P_{MT}, and R_{MT} denote, respectively, the newly installed microturbine each year (%), power produced by the microturbine (kW), and price of the microturbine ($/kW). The operational and maintenance cost of the wind power system (C^{MT}_{op}) is expressed based on [48] as

$$C^{MT}_{op} = \sum_{y\in Y}\left(MT^{y}_{p} \times O_{MT} \times N_{P1} \times 365\right), \tag{6}$$

where MT^{y}_{p} and O_{MT} denote, respectively, the power produced by microturbine (kW) and operational cost of microturbine ($/kW). The investment cost of converters (C^{inv}_{con}) used for ESS is expressed as

$$C^{inv}_{con} = \sum_{y\in Y}\left(NC^{y}_{con} \times P_{con} \times R_{con} \times N_{eq} \times N_{P1}\right), \tag{7}$$

where NC^{y}_{con} is the newly installed for ESS each year, P_{con} is the rated power of the converter for ESS, and R_{con} represents the price of converter for ESS, respectively. The operational and maintenance cost of the converter for ESS is expressed as

$$C^{con}_{op} = \sum_{y\in Y}\left(NCT^{y}_{con} \times P_{con} \times O_{con} \times N_{P1} \times 365\right), \tag{8}$$

where NCT^{y}_{con} and O_{con} are the available power of the converter of the year and operational cost of the converter system ($/year), respectively. The investment cost (C^{ESS}_{inv}) related to expanding the ESS can be expressed as

$$C^{ESS}_{inv} = \sum_{y\in Y}\left(NC^{y}_{ESS} \times P_{ESS} \times R_{ESS} \times N_{eq} \times N_{P1}\right), \tag{9}$$

where NC^{y}_{ESS} is the new capacity of ESS installed each year (%), P_{ESS} is the rated capacity of the ESS (kWh), and R_{ESS} is the price of ESS ($/year). The operational cost of the ESS is given by

$$C^{ESS}_{op} = \sum_{y\in Y}\left(NCT^{y}_{ESS} \times P_{ESS} \times O_{ESS} \times N_{eq} \times 365\right), \tag{10}$$

where NCT^{y}_{ESS} is the available capacity of ESS each year (%) and O_{ESS} is the operational cost of the capacity of ESS ($/year). The objective function (F) for the EVCS expansion can be expressed as

$$\begin{aligned} \text{Min}\,(F) = {} & C^{PV}_{cost} + C^{PV}_{op} + C^{WP}_{cost} + C^{WP}_{op} + C^{MT}_{cost} + C^{MT}_{op} \\ & + C^{inv}_{con} + C^{con}_{op} + C^{ESS}_{inv} + C^{ESS}_{op} + C^{L}_{in}, \end{aligned} \tag{11}$$

where C^{L}_{in} is the investment cost of the land required for installing the wind and solar systems.

3.2.1. Constraints Used in This Model. Various constraints have been used to estimate the proposed expansion planning. The planning horizon of the solar power installation at each stage is signified by

$$\left.\begin{aligned} NI^{y}_{PV} &= PV^{y}_{a} - NI^{y-1}_{PV} \\ NI^{y}_{PV} &\le L_{PV1} \\ PV^{y}_{a} &\le L_{PV2} \end{aligned}\right\} \forall\ y \in Y, \tag{12}$$

where NI^{y}_{PV}, L_{PV1}, and L_{PV2} are the new solar PV system installation each year, constraints on installing the new solar

PV power each year, and limitation on installing the new solar PV power during the consecutive year, respectively. The proposed expansion model expands the power and capacity of ESS by including its rated power. It can be expressed based on [45] as

$$\left.\begin{aligned} NC_{con}^{y} &\le L_{con1} \\ NCT_{con}^{y} &\le L_{con2} \end{aligned}\right\} \forall\ y \in Y. \tag{13}$$

The capacity of ESS is expanded by considering the following constraints:

$$\left.\begin{aligned} NC_{ESS}^{y} &= NCT_{ESS}^{y} - NCT_{ESS}^{y-1} \\ NCT_{ESS}^{y} &\le L_{ESS1} \\ NCT_{ESS}^{y} &\le L_{ESS2} \end{aligned}\right\} \forall\ y \in Y, \tag{14}$$

where L_{ESS1} and L_{ESS2} are the constraint on installing the new storage capacity each year and the limitation on installing the new storage capacity during consecutive years, respectively. In the proposed model, the short-term plan is improved using optimization for getting a long-term extension plan. The resources such as ESS, solar PV system, and water electrolyzer are optimized. The charging and discharging pattern of ESS are given by

$$\left.\begin{aligned} P_{CH}^{s,t,y} \times b_{CH}^{s,t,y} &\le P_{con} \\ P_{DC}^{s,t,y} \times b_{DC}^{s,t,y} &\le P_{con} \\ b_{CH}^{s,t,y} + b_{DC}^{s,t,y} &\le 1 \end{aligned}\right\} \forall\ s \in S,\ t \in T, y \in Y,$$

$$\left.\begin{aligned} SE_{ESS}^{s,t,y} &\le C_{ES} \\ SE_{ESS}^{s,t,y} &= SE_{ESS}^{s,t,y-1} + P_{CH}^{s,t,y} - P_{DC}^{s,t,y} \end{aligned}\right\} \forall\ \forall\ s \in S,\ t \in T, y \in Y, \tag{15}$$

$$\eta_{ESS} = \frac{\sum_{t\in T} P_{DC}^{s,t,y}}{\sum_{t\in T} P_{CH}^{s,t,y}},\quad \forall\ s \in S,\ y \in Y,$$

where $P_{CH}^{s,t,y}$ is the charged power of the ESS (kW), the superscript s,t,y indicates the yearly short-term plan, $b_{CH}^{s,t,y}$ is the binary variable related to the charging state of ESS, $P_{DC}^{s,t,y}$ is the discharged power from the ESS (kW), $b_{DC}^{s,t,y}$ is the binary variable related to the discharging state of ESS, $SE_{ESS}^{s,t,y}$ is the stored energy in ESS (kWh), C_{ES} is the rated capacity of energy storage (kWh), η_{ESS} is the efficiency of ESS (%), s is the index of scenarios, S is the set of scenarios, t is the index of hours, and T is the set of hours. Energy of each EV ($E_{EV}^{v,t,y}$) in the charging station is given by

$$\left.\begin{aligned} E_{EV}^{v,t,y} &= E_{EV}^{v,t,y-1} + E_{CEV}^{v,t,y} - E_{DEV}^{v,t,y} \\ E_{EV}^{v,t,y} &\le C_{EV} \end{aligned}\right\} \forall\ v \in V,\ t \in T, y \in Y, \tag{16}$$

where $E_{CEV}^{v,t,y}$ is the charged energy to EVs (kW), $E_{CEV}^{v,t,y}$ is the discharged energy from ESS (kW), and C_{EV} is the rated capacity of EVs (kWh). The total charged power and discharging power of the charging station are given by

$$\left.\begin{aligned} P_{CH}^{s,t,y} &= \sum_{n\in N} P_{CEV}^{v,t,y} \\ P_{CH}^{s,t,y} &= \sum_{n\in N} P_{DEV}^{v,t,y} \end{aligned}\right\},\ \forall\ t \in T, y \in Y. \tag{17}$$

In the proposed expansion model, the short-term plan optimizes the hourly operation of the BESS, EVs, and microturbine. On the other hand, the long-term plan installs new capacity of ESS, solar PV system, wind, and microturbines. This coordination provides optimized output.

3.2.2. Operating Conditions. The objective function devised in the prior subsection is minimized in agreement with some equality and inequality constraints. The power flow balance equation is expressed using the equality constraints as follows:

$$\begin{aligned} P_{aj} - P_{mj} - V_j \sum_{k=1}^{N_b} V_k Y_{jk} cos\left(\beta_j - \beta_k - \varphi_{jk}\right) = 0, \\ Q_{aj} - Q_{mj} - V_j \sum_{k=1}^{N_b} V_k Y_{jk} cos\left(\beta_j - \beta_k - \varphi_{jk}\right) = 0, \end{aligned} \tag{18}$$

where P_{ai}, P_{mj}, V_j, N_b, V_k, Y_{jk}, β_j, β_k, $an\ d\ \mu_{jk}$, denote, respectively, the active power generation of j-th bus, the active power demand of j-th bus, the voltage of j-th bus, the total number of buses of the distribution network, the magnitude of (i, j)-th term of bus admittance matrix, the voltage angle of j-th bus, the voltage angle of k-th bus, and the angle of Y_{ij}. $Q_{aj} an\ d\ Q_{mj}$ are the reactive power generation of j-th bus and reactive power demand of j-th bus, respectively.

The minimum and maximum number of slow and fast and charging stations placed at the candidate locations are given by

$$\begin{aligned} 0 < N_{Sk} \le m_{scs}, \\ 0 < N_{Fk} \le m_{fcs}, \end{aligned} \tag{19}$$

where N_{Sk}, m_{scs}, N_{Fk}, $an\ d\ m_{fcs}$ are the number of slow charging stations at bus k, the maximum number of slow charging stations that can be placed at a particular bus, the number of slow charging stations at bus k, and the maximum number of fast-charging stations that can be placed at a particular bus, respectively.

The lower and upper limit of reactive power and the maximum safe limit of load are given by

$$\begin{aligned} Q_{min} < Q_j \le Q_{max}, \\ L_d \le L_{dmax}, \end{aligned} \tag{20}$$

where Q_{min}, Q_{max}, $an\ d\ L_{dm\ ax}$ denote, respectively, the lower bound of reactive power limit of each bus, the upper bound of reactive power limit of each bus, and the loading margin of the network.

3.3. Waiting Time of EV. When the arrival rate of the EVs is lesser than the service rate, no queue will be formed in the charging station. In this study, deterministic queuing is considered [50]. When several vehicles exceed the hourly charging limit of the charger, the extra EVs have to wait. By considering the right triangle waiting time function, the area of the triangle is equal to the total queue time of the EV charging station. The number of users has been taken on one side of the triangle, and the waiting time of the last EV has been taken on the other side. The waiting time of the last EV is the difference between the rate of service and the rate of arrival multiplied by the average charging time. The total queuing time of EV can be expressed as

$$T_q^n = 0.5T_o t_q^n y_q^n \left(\delta_q^n - \mu_q^n\right), \ \forall\ n \epsilon N, \tag{21}$$

where $T_o, t_q^n an\ d\ y_q^n$ denote, respectively, the design period, the recharging time of the q-th recharging station for the n-th class (class represents the type of storage system used in the EV), and the total number of EVs visiting the q-th recharging station. δ_q^n is the arrival rate (average number of EVs visiting each charger in a station per hour). μ_q^n is the rate of service (average number of EVs served by each charger in a station per hour).

3.4. Formulation of CNN-DCE. The architecture of CNN contains an input layer, convolution layer, ReLU layer, maximum pooling layer, fully connected layer, and output layer. By using convolution kernels, features were extracted from the input signal through the convolution layer. By using gradient descent training, the weights of the convolution layer were optimized, which in turn adjusted the convolution layer parameters. The extracted features from the convolution layer were mapped into feature space using the ReLU layer. The dimensions of the mapped features were reduced by the pooling layer, which included max-pooling and average pooling, which has no weights or bias to train the CNN. The function f illustrates the objective function of CNN-DCE; it should be minimized. It is expressed as

$$f(G) = \left(C_{cost}^{PV},\ C_{op}^{PV}, C_{cost}^{WP},\ C_{op}^{WP},\ C_{cost}^{MT},\ C_{op}^{MT}, C_{con}^{inv}, C_{op}^{con}, C_{inv}^{ESS}, C_{op}^{ESS},\ T_q^n, C_{in}^{L}\right), \tag{22}$$

where C_{cost}^{PV}, C_{cost}^{WP}, and C_{cost}^{MT} represent the investment cost of the solar PV system, wind turbine system, and microturbine, respectively. $C_{op}^{PV}, C_{op}^{WP}, C_{op}^{MT}, C_{op}^{con}$, and C_{op}^{ESS} denote, respectively, the operational and maintenance cost of the solar PV system, wind turbine system, microturbine, converter, and ESS. C_{con}^{inv} and C_{inv}^{ESS} denote the investment cost of converters and investment cost related to expanding the ESS, T_q^n is the total queuing time of EVs, and C_{in}^{L} is the investment cost of the land required for installing the wind and solar systems.

As shown in Figure 6, each CNN model structure has 10 input variables: C_{cost}^{PV}, $C_{op}^{PV}, C_{cost}^{WP}$, C_{op}^{WP}, C_{cost}^{MT}, C_{op}^{MT}, C_{con}^{inv}, $C_{op}^{con}, C_{inv}^{ESS}, C_{op}^{ESS}$. After the CNN model was established, the training toolbox (trainbr) was used to minimize the performance index between the input and output by adjusting the weights. The performance of the proposed CNN-DCE is evaluated using five statistical error criteria: mean squared error (MSE), mean absolute error (MAE), correlation coefficient (R), and scatter index (SI). The MSE is expressed based on [45] as

$$MSE = \frac{1}{M}\sum_{j=1}^{M}\left(E_j - P_j\right)^2, \tag{23}$$

where M, E, and P denote, respectively, the number of experiments, the experimental value, and the predicted value. Once the CNN models are correctly trained, the optimal network is selected using the correlation coefficient between the target output and the network output. The R value is expressed based on [51] as

$$R = \frac{(E - \overline{E})(P - \overline{P})^T}{\sqrt{(E - \overline{E})(E - \overline{E})^T}\sqrt{(P - \overline{P})(P - \overline{P})^T}}, \tag{24}$$

where $\overline{E} an\ d\ \overline{P}$ represent the average of the experimental value and the average of the predicted value, respectively. MAE is the average of the disparity between the predicted values and the original values. It is used to assess how far the actual output is from the predicted values. Mathematically, it is expressed as

$$MAE = \frac{1}{M}\sum_{j=1}^{M}\left|E_j - P_j\right|. \tag{25}$$

SI is close to RMSE. Mathematically, it is expressed as

$$SI = \sqrt{\frac{1}{M}\sum_{j=1}^{M}\left(E_j - P_j\right)^2}/\overline{E_j} \times 100. \tag{26}$$

The scatter plot of the output of CNN versus the test data is shown in Figure 7. It is observed that the selected CNN provides good generalization ability because their R values are very close to one.

The statistical performance of the proposed CNN-DCE is assessed with three different machine learning algorithms, such as K-nearest neighbor (KNN), artificial neural networks (ANN), and support vector machine (SVM). Table 1 shows the training and testing results. It is observed from Table 1 that the SVM is very close to the proposed CNN-DCE in a few cases. On the whole, CNN-DCE provides better performance than SVM, ANN, and KNN. Therefore, CNN is selected in this study.

4. Experiments

4.1. Training. For estimating the capacity expansion problem, optimized CNN was used. Nine different datasets of renewable sources were taken from [52,53]. The solar dataset

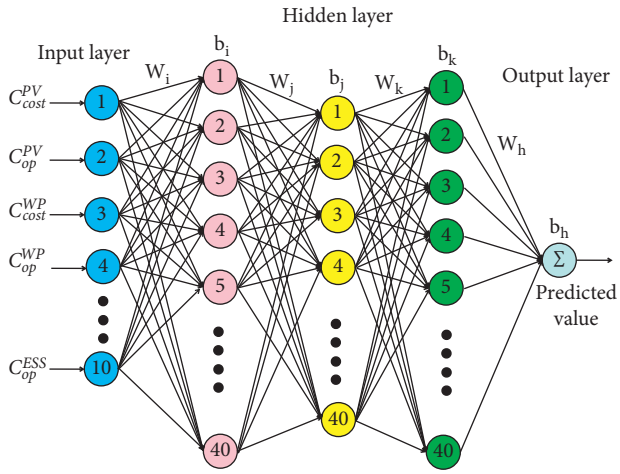

Figure 6: CNN model for the proposed DCE problem.

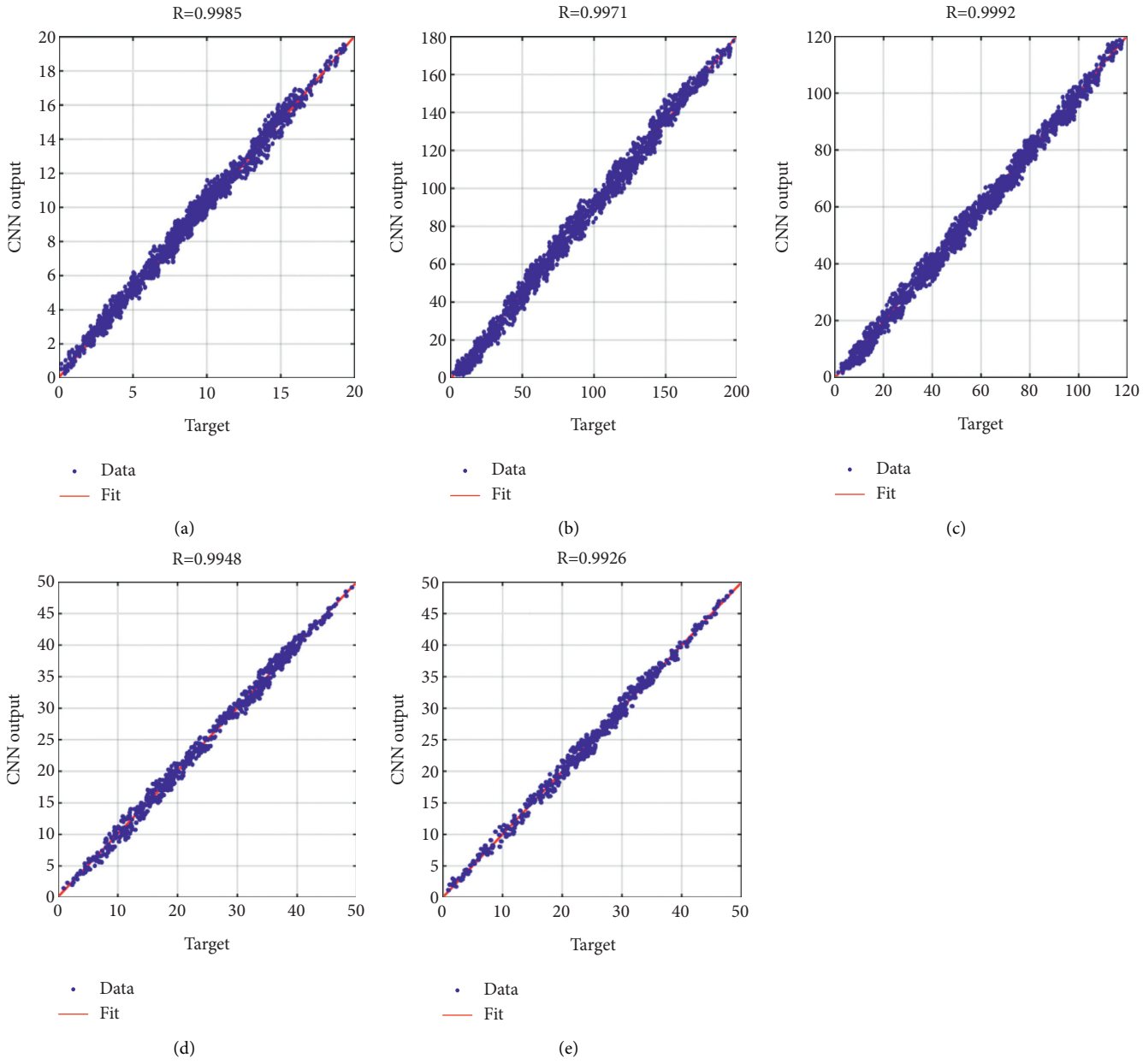

Figure 7: Output of CNN versus target values for test datasets. (a) Solar power, (b) wind power, (c) microturbine power, (d) BESS charging, and (e) BESS discharging.

has different attributes, such as solar power per hour and cumulative power generation per day. The wind dataset contains wind speed, wind direction, active power, and output power per hour. There are 68,779 data, and 50,531 data are available in solar and wind energy, respectively, for dataset-1. There are 490 data from the solar dataset, and 495 data from the wind dataset have been selected. To test the performance of CNN, 20% of the data were randomly selected from the total, the remaining 80% of data were used for training, and the collected datasets are listed in Table 2. Similarly, the data from the other eight datasets have been chosen randomly (Table 2). The rating of BESS was selected based on the peak loading and the requirement of the system. In this paper, 5.2 kW BESS was selected for handling the peak load of 5 kW.

The training error was estimated using RMSE. The acquired datasets were applied to CNN, and the estimated error during training is shown in Figure 8. The RMSE of each neuron of the hidden layer gets varied throughout the training. In this study, we assessed the performance of neurons from 2 to 10. It was observed that a minimal RMSE value was obtained from the 6th neuron, while the RMSE decreased tediously from the 2nd to 6th neurons and increased from the 6th to 10th neuron (Figure 8). Thus, the 6th neuron provided an accurate estimation of the capacity expansion problem. As a result, 60-fold iterated 6-neuron CNN was used in this study.

4.2. Testing. To test the performance of the proposed design, indices such as RMSE, MAE, OIM, and COV were used. Various parameters of different algorithms are listed in Table 3. The obtained datasets were applied to the proposed CNN, and the numerical test was conducted (Table 4). According to the obtained results, the proposed CNN-DCE (dataset-I) provided better performance with RMSE = 0.52, MAE = 0.44, OIM = 0.94, and COV = 0.96, followed by FOT (RMSE = 0.68, MAE = 0.55, OIM = 0.86, and COV = 0.85) for training. Comparing the proposed CNN-DCE with FOT, RMSE = 26.7%, MAE = 22.2%, OIM = 8.8%, and COV = 12.15% were achieved. The performance index of the PSO was the worst compared to CNN-DCE and FOT in the capacity expansion problem.

During training, a learning rate of 0.01 and a maximum of 26 epochs were used for better learning. Each epoch used 31 iterations with a maximum of 806 iterations. The training progress plot of CNN without optimization is shown in Figure 9. While plotting, several iterations were taken on the x-axis, and the training accuracies and losses were taken on the y-axis. From Figure 9, one can easily understand that the validation accuracy of 90.80% was obtained during the training progress. The experiment was performed using Matlab software, and the entire training took 1 minute and 54 seconds.

The accuracy of CNN belongs to its hyperparameters. In this study, the hyperparameters were optimized using the FPOA algorithm. The dataset was trained with a learning rate of 0.01. During the optimized training process, a total of 26 epochs, each with 31 iterations, were used with a maximum iteration of 806. The accuracy and loss plot for the optimized CNN are shown in Figure 10. The obtained result shows that the validation accuracy was 98.30%. Comparing Figures 9 and 10 (nonoptimized CNN with optimized CNN), the proposed optimized CNN provided an improved accuracy by 8.15%.

5. Results and Discussion

5.1. Test Case. A microgrid combined with 10 kW microturbines, solar panels, and 40 kW wind turbines can be used as a test case. 200 kW is considered the load demand peak. The power of the energy storage device is 10 kW, and the capacity is 30 kWh. A 175 kW line is used to connect the microgrid to the upstream grid. Fuel required for microturbine costs around 0.2$/kWh [40]. Table 5 shows the operational and investment costs of all the energy sources. Wind and solar systems have a life span of 8 years, whereas for microturbine and BESS, it is 6 years.

EVCS are connected to the microturbine, and they can charge the vehicles at a charging rate of 100 kW. The charging capacity of EV is 100 kWh, and it uses the technology of vehicle-to-grid charging. Moreover, the CS can charge up to three vehicles simultaneously. Table 6 shows the load, cost of energy, and the hourly profile for wind and solar energy. The planning boundary is considered to be 5 years, and Figure 11 shows the growth of the load and fuel prize over this span of years. Each capacity resource can be expanded with some limitations. It is expanded to 100% at each stage, and the overall expansion of each capacity resource over the planning boundary is 150%.

A microgrid is used as a case study to simulate the specified method for expanding the capacity. All the microgrid resources are capacity expanded. The long-term expansion plan results are shown in Table 7. In order to cope with the growth in load demand, the specified model uses different resources in different years of the planning boundary. The expansion of wind energy is needed more when compared to solar energy as the profile of wind energy is wider. Since the wind system provides more energy to the microgrid, more wind turbines are used in the microgrid. In the final year of the planning boundary, a microturbine is installed to supply the load growth. The power and capacity of the energy storage devices are expanded in different years of planning boundary. To improvise the model, energy storage devices cut the peak load and shift the energy over the hours. Hence, more energy storage devices are installed in the microgrid.

The annual expansion cost of all the resources and the overall cost for planning are shown in Table 8. The investment cost of wind energy covers most of the cost. Wind power contributes to 56% of the planning cost, and the installation of a microturbine in the 5th year contributes to 22% of the total cost. Solar power and energy storage devices contribute to the remaining cost. The specified expansion plan optimizes the operation of energy storage devices and microturbine to reduce the new technology investment cost. The microturbine operation in the five years of the planning horizon is shown in Figure 12.

Table 1: Statistical performance of the proposed CNN-DCE and other techniques during training and testing.

Input/model	Training				Testing			
	MAE	MSE	SI	R	MAE	MSE	SI	R
KNN	0.388	0.956	0.250	0.933	0.430	0.930	0.291	0.941
ANN	0.373	0.986	0.236	0.942	0.413	0.951	0.274	0.962
SVM	0.295	0.944	0.155	0.910	0.332	0.941	0.221	0.963
CNN-DCE	0.263	0.930	0.145	0.907	0.321	0.925	0.230	0.931

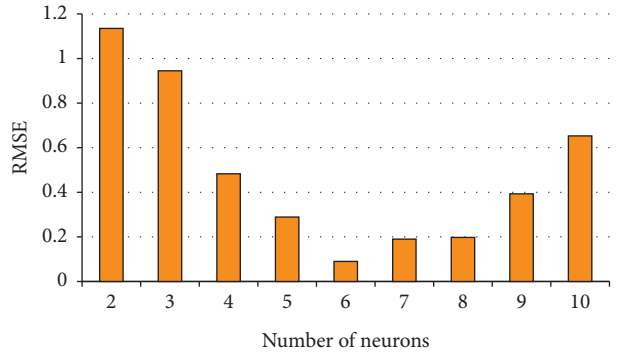

Figure 8: RMSE of different neuron numbers for the test dataset on capacity expansion problem.

Table 2: Training and testing report of nine different datasets.

Datasets	Solar dataset	Wind dataset	Total dataset	Number of data used	
				Training	Testing
Set -1	490	495	985	821	164
Set -2	355	352	707	589	118
Set -3	500	419	919	766	153
Set -4	321	340	661	551	110
Set -5	452	466	918	765	153
Set -6	640	640	1280	1067	213
Set -7	500	514	1014	845	169
Set -8	762	755	1517	1264	253
Set -9	575	572	1147	956	191

Table 3: Various parameters of different algorithm used for simulation.

Algorithm	Parameters	Value
PSO	$c1$, $c2$	1.49445
	w	0.729
FFO	ax, ay	20, 20
	bx, by	10, 10
FOT	φ, α,	0.05, 0.5,
	$\beta_{\min}$, λ	0.2, 1.0
FPOA	λ	1.5
	ρ	0.8

When the peak load occurs at hours 15–21, the microturbine starts to operate. The operation of the microturbine in 1 to 5 years is not important because most of the supply is contributed by wind and solar energy. The microturbine is used only at certain hours when there is a shortage. A microgrid needs more power during the final year when load growth is high. Hence, to supply more energy in the last year, the microturbine works at the highest capacity.

Figure 13 shows the power exchange between the upstream grid and microgrid for the five-year planning of a day. The maximum line capacity between the upstream grid and microgrid is 175 kW. Due to this limitation, growth in the load can be supplied by installing other capacity resources like BESS, solar wind, and microturbine. Apart from installing the additional capacity resources, the proposed model also optimizes microturbine and energy storage devices operating simultaneously. BESS operation for different

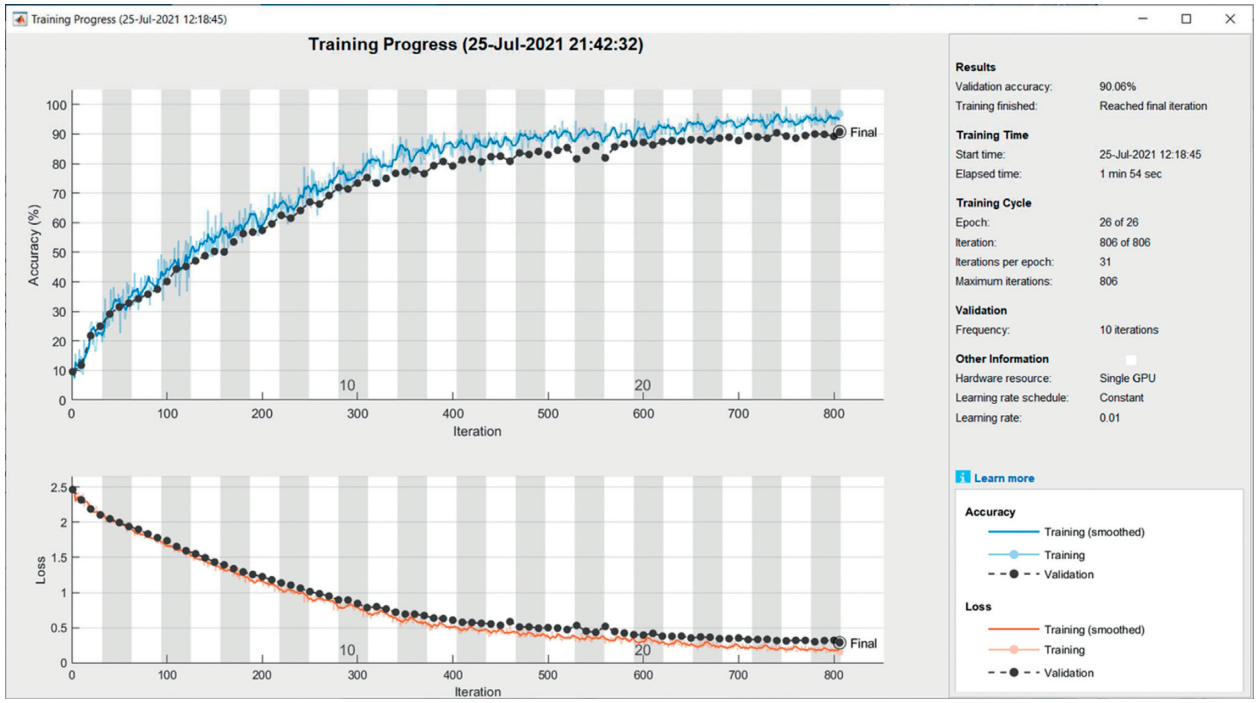

Figure 9: Training progress plots of CNN without optimization.

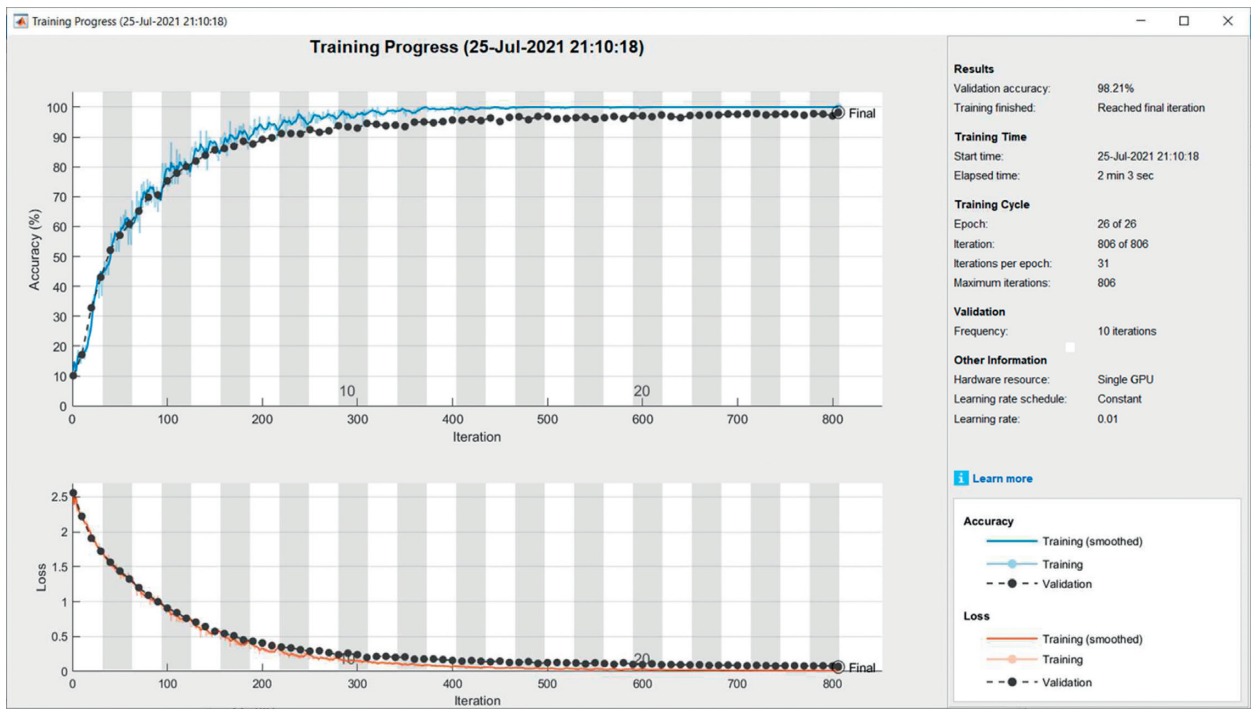

Figure 10: Training progress plots of CNN with optimization.

years of planning boundary is shown in Figure 14. It automatically shifts the energy to the higher price hours from the lower price hours, managing the peak load.

The optimized operation of EVCS is performed by the proposed planning. EVCS use the technology of vehicle-to-grid for charging EVs. The flexible operation of CS is achieved by optimizing the operation of EVs. Any EV is taken to discuss the performance of the CS. For example, Figure 15 shows that an EV comes to a CS with 10 kWh of initial energy at hour 17. It is fully charged at hour 18 and then discharges the power to the microgrid at hour 20. Then it is fully charged at hour 20 before leaving the EVCS. This process is optimized for all the vehicles that visit the EVCS and make the CS transfer power to the microgrid. Table 9

Table 4: Performance on training and testing the nine datasets.

	Algorithm	RMSE		MAE		OIM		COV	
		Training	Test	Training	Test	Training	Test	Training	Test
Dataset-1	PSO	0.96	0.85	0.81	0.85	0.53	0.43	0.81	0.78
	FFO	0.89	0.76	0.72	0.64	0.71	0.58	0.87	0.72
	FOT	0.68	0.43	0.55	0.68	0.86	0.71	0.85	0.83
	CNN-DCE	0.52	0.32	0.44	0.34	0.94	0.83	0.96	0.89
Dataset-2	PSO	0.89	0.71	0.88	0.80	0.61	0.46	0.85	0.81
	FFO	0.84	0.84	0.71	0.68	0.78	0.59	0.89	0.75
	FOT	0.41	0.32	0.52	0.57	0.89	0.76	0.93	0.81
	CNN-DCE	0.28	0.20	0.39	0.37	0.96	0.87	0.97	0.90
Dataset-3	PSO	0.89	0.98	0.92	0.89	0.58	0.51	0.85	0.78
	FFO	0.91	0.68	0.78	0.76	0.79	0.54	0.82	0.84
	FOT	0.48	0.43	0.71	0.69	0.91	0.78	0.95	0.88
	CNN-DCE	0.24	0.25	0.60	0.52	0.97	0.85	0.98	0.92
Dataset-4	PSO	0.92	0.90	0.80	0.76	0.60	0.47	0.83	0.79
	FFO	0.73	0.70	0.71	0.65	0.78	0.59	0.85	0.77
	FOT	0.64	0.59	0.53	0.50	0.89	0.76	0.93	0.85
	CNN-DCE	0.57	0.50	0.40	0.30	0.98	0.89	0.97	0.93
Dataset-5	PSO	0.89	0.86	0.84	0.72	0.54	0.44	0.82	0.77
	FFO	0.87	0.77	0.75	0.64	0.73	0.59	0.86	0.75
	FOT	0.39	0.36	0.58	0.53	0.87	0.74	0.93	0.81
	CNN-DCE	0.30	0.26	0.47	0.40	0.95	0.85	0.95	0.92
Dataset-6	PSO	0.88	0.85	0.87	0.86	0.57	0.45	0.80	0.79
	FFO	0.84	0.84	0.76	0.67	0.75	0.59	0.85	0.71
	FOT	0.41	0.37	0.65	0.58	0.89	0.73	0.91	0.85
	CNN-DCE	0.27	0.26	0.31	0.30	0.95	0.84	0.95	0.91
Dataset-7	PSO	0.81	0.84	0.92	0.74	0.74	0.53	0.83	0.73
	FFO	0.70	0.73	0.79	0.65	0.63	0.64	0.88	0.69
	FOT	0.47	0.45	0.32	0.28	0.88	0.70	0.94	0.82
	CNN-DCE	0.30	0.25	0.24	0.22	0.97	0.87	0.97	0.93
Dataset-8	PSO	0.84	0.76	0.96	0.95	0.58	0.48	0.77	0.84
	FFO	0.73	0.70	0.84	0.82	0.64	0.62	0.84	0.73
	FOT	0.55	0.54	0.47	0.39	0.79	0.80	0.91	0.84
	CNN-DCE	0.42	0.34	0.21	0.19	0.93	0.91	0.98	0.93
Dataset-9	PSO	0.94	0.21	0.92	0.83	0.63	0.48	0.85	0.75
	FFO	0.98	0.44	0.80	0.78	0.78	0.62	0.89	0.80
	FOT	0.42	0.33	0.44	0.39	0.84	0.75	0.93	0.79
	CNN-DCE	0.31	0.25	0.27	0.20	0.93	0.89	0.98	0.90

Table 5: The investment and operational cost of various energy resources of charging station.

	Resources				
	Solar power	Wind power	Microturbine	BESS capacity	BESS power
Investment cost	1300 ($/kW)	2000 ($/kW)	600 ($/kW)	400 ($/kWh)	400 ($/kW)
Functional and maintenance cost ($/kWh)	0.1	0.1	0.25	0.1	0.1

shows the power injected by EVCS into the microgrid for the five-year planning horizon. Usually, power injection to the microgrid takes place when the price of the energy is high.

5.2. Impacts of Charging Station on Expansion Plan. As the process of charging the EVs is optimized, the CS acts as a flexible load on the microgrid. At some point in time, the vehicle-to-grid method makes the CS act like a generating unit. The proposed model is simulated without a vehicle-to-grid method to signify the importance of CS in the proposed plan, and the result is shown in Table 10. There is a 31% increase in the overall cost of expansion. The expansion of resources such as BESS, microturbine, solar, and wind energy system is listed in Table 11.

It shows that, to cope with the growth of the load, the microgrid requires huge capacity resources and the microturbine and especially requires larger expansion. Table 12 compares the result of using the vehicle-to-grid method to not using the vehicle-to-grid method. This clearly shows that about a 72 kW larger microturbine is needed by a microgrid, which does not use vehicle-to-grid technology.

5.3. The Parametric Uncertainty. Parametric uncertainty is considered in the proposed model. Figure 16 shows the

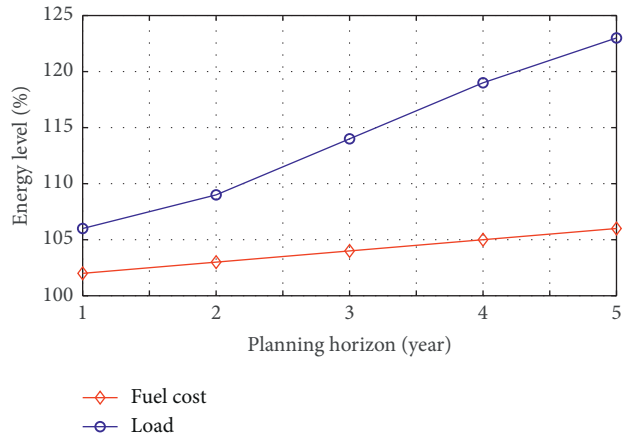

Figure 11: Growth of the load and fuel price for the proposed planning horizon.

Table 6: Hourly profile of different resources of EVCS.

Hours	1	2	3	4	5	6	7	8	9	10	11	12	13	14	15	16	17	18	19	20	21	22	23
Solar power (%)	0	0	0	0	0	9	14	23	48	62	88	100	100	94	75	52	37	14	5	0	0	0	0
Wind power (%)	72	80	70	76	80	82	81	70	65	50	44	48	32	30	42	55	43	65	82	100	87	76	71
Load power (%)	9	10	7	10	11	9	18	29	35	53	67	65	70	75	83	87	84	92	100	97	80	50	35
Electricity price ($/kWh)	10	10	10	10	10	10	10	10	15	15	15	15	15	15	15	20	20	20	20	20	20	15	15

Table 7: Results of expansion of different energy resources.

	Resources				
	Solar power (%)	Wind power (%)	Microturbine (%)	BESS capacity (%)	BESS power (%)
Year-1	—	90	—	—	70
Year-2	—	40	—	55	45
Year-3	21.5	—	—	35	—
Year-4	—	30	—	20	—
Year-5	—	—	42	—	24

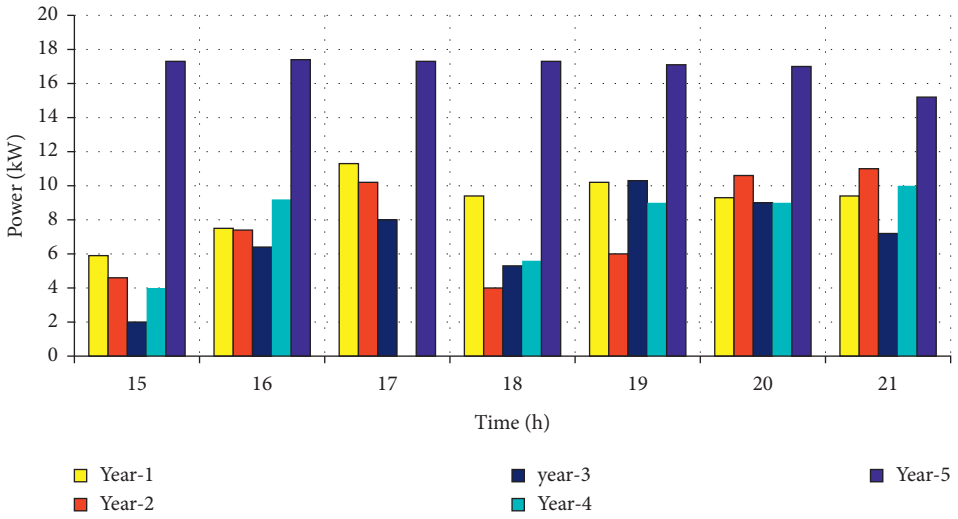

Figure 12: Operation of microturbine during the five-year planning.

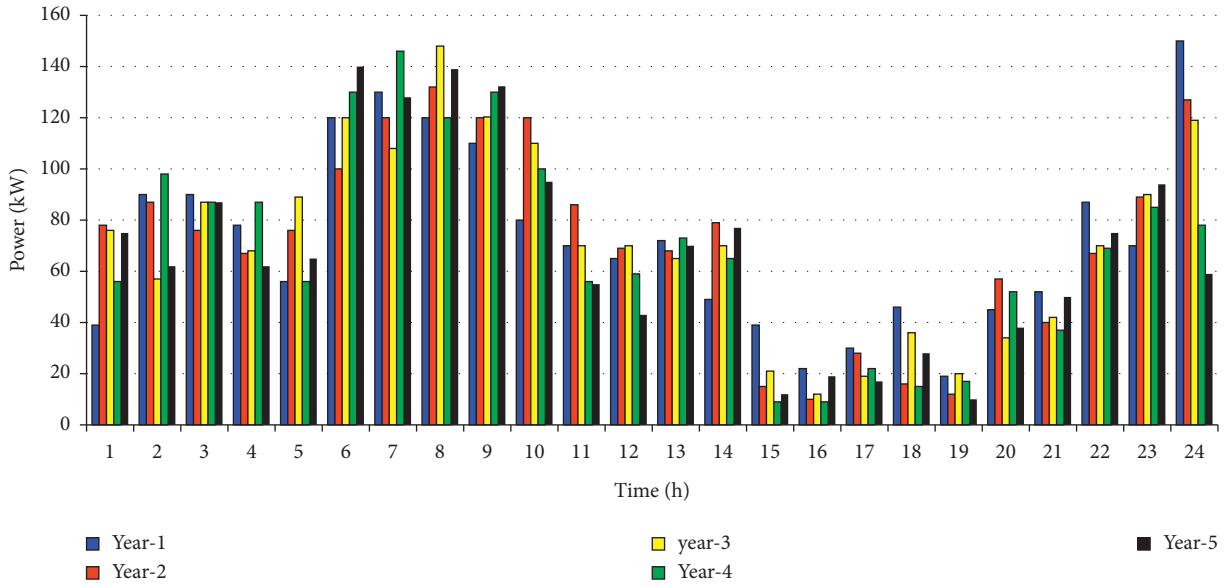

Figure 13: Exchanged power between microgrid and upstream network for the five-year planning.

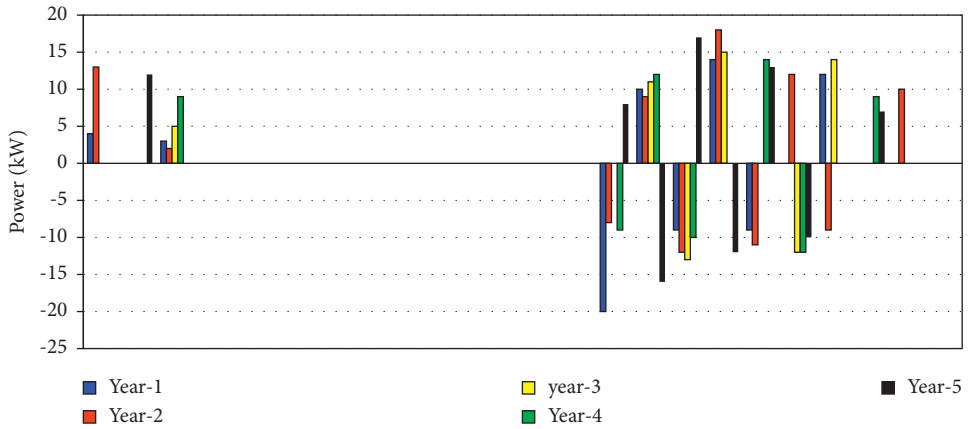

Figure 14: Operation of BESS in the five-year planning horizon.

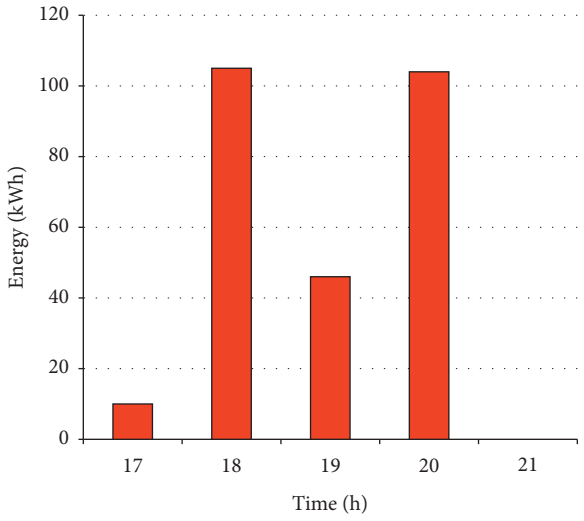

Figure 15: EV arrived at hour 20 with a 10 kW charge.

Table 8: Annual expansion cost for all the energy resources.

	Resources					
	Solar power	Wind power	Microturbine	BESS capacity	BESS power	Total cost (%/year)
Annual expansion cost ($/year)	1580.56	22516.87	8910.21	6540.12	953.25	40500.01

Table 9: Injected power to the microgrid by an EVCS in a day of a five-year planning horizon.

Hours	1	5	6	7	11	12	15	17	20	22	23
Year-1	113	0	0	0	21.7	0	23.4	0	102	87.3	105.2
Year-2	0	47.2	26.7	0	7.3	0	20.8	0	0	92.7	76.9
Year-3	0	0	12.4	37.2	0	0	0	0	0	0	0
Year-4	29	110.3	0	0	0	28.4	0	38.9	67.2	0	62.3
Year-5	0	0	23.6	18.6	32.4	11.7	29.4	0	89.1	53.2	0

Table 10: EV without vehicle-to-grid technique for the expansion plan.

	Resources					
	Solar power ($)	Wind power ($)	Microturbine ($)	BESS capacity ($)	BESS power ($)	Total cost ($)
Annual expansion cost ($/year)	1693.17	22835.83	20016.73	7603.18	1024.92	53173.83

Table 11: Percentage of resources expanded without vehicle-to-grid technique.

	Resources				
	Solar power (kW)	Wind power (kW)	Microturbine (kW)	BESS capacity (kWh)	BESS power (kW)
Year-1	—	100	—	—	76
Year-2	—	40	10.35	55	45
Year-3	21.5	—	61.87	35	—
Year-4	—	50	—	20	—
Year-5	—	—	42	—	24

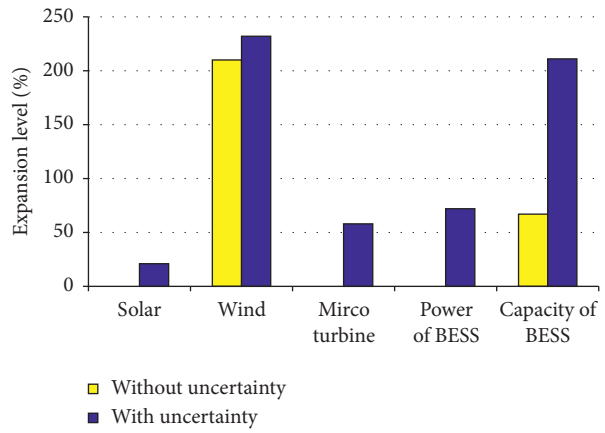

Figure 16: Various capacity resources without uncertainty and including uncertainty for the expansion plan.

expansion with and without uncertainty. For the model with uncertainty, the microgrid requires larger and high-capacity resources, whereas for the model without uncertainty, to supply for the load growth, the microgrid requires small and fewer capacity resources. Figure 17 shows the power shared by various capacity resources to meet the demand at one particular hour. Various resources supply the microgrid load together. For example, at hour 19, capacity resources supply 30% of the required energy, and the balance of the required energy is supplied by the upstream network. At this point in time, power supplied by solar energy is zero, and it does not contribute much to the microgrid.

It is necessary to distribute the load evenly on the three-phase power system to avoid different voltage drops between different phases. It is to be noted that, in the two cases, a highly uneven distribution of EV load in the LV distribution network leads to unbalance voltage problem. This problem can be efficiently handled by the proposed CNN-DCE by including the TOU tariff rate technique, BESS, and including renewable sources. For the TOU tariff, the CNN-DCE shifts

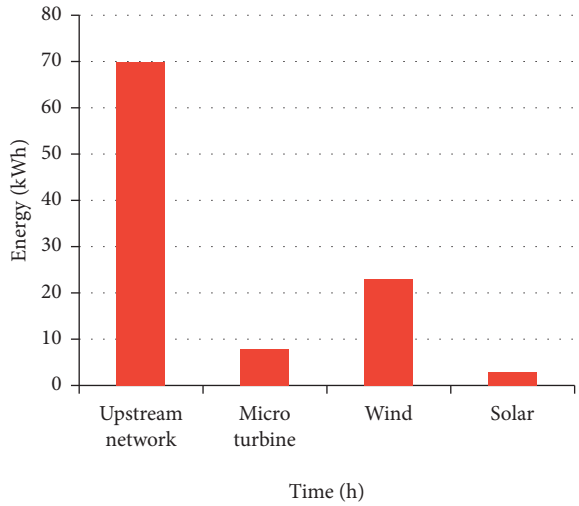

Figure 17: Power shared by various capacity resources at hour 19.

Table 12: Comparison between vehicle-to-grid and without vehicle-to-grid technique for the expansion plan.

Resources	Capacity installed		Cost ($/year)	
	With vehicle-to-grid	Without vehicle-to-grid	With vehicle-to-grid	Without vehicle-to-grid
Solar power (kW)	20.25	20.25	1580.56	1674.92
Wind power (kW)	210	210	21538.53	21724.73
Microturbine (kW)	56.39	128.42	8935.25	18482.39
BESS (kW)	72	61.5	953.25	841.71
BESS capacity (kW)	210	210.2	7493.34	7612.96
Total cost of expansion ($/year)			40,500.01	50336.71

the load in on-peak duration to the off-peak and medium-peak durations. As a result, the load can be shared, and unbalance can be avoided. Similarly, incorporating more BESS and renewable sources (wind and solar) can avoid the peak load. Thus, unbalance can be avoided.

5.4. Numerical Study. By considering the demand variability, in this study, five datasets were generated (Day-1 to Day-5) with 900, 1350, 1100, 1000, and 1200 customers over 24 h, respectively. Based on the probability of trip occurrence, the data is sampled randomly from the Luxmobil survey. Each dataset has five test instances. As each sampled trip has the departure time, the hourly trip is estimated, and the interarrival time is generated using the Poisson distribution. The charging infrastructure considered in this study comprises the public Chargy network and fifteen DC fast chargers. The *k*-means clustering method was used to estimate the location of the charging station near the drop-off locations of customers [48]. The results of the proposed CNN-DCE and three other state-of-the-art methods are listed in Table 13.

It is observed that the ANN and CNN-DCE provide lower average waiting times (2.4 and 0 min) than KNN and SVM (4.6 and 3.8 min) for Day-1 operation. A total of 900 vehicles have taken part during the charging operation. Similarly, the ANN and CNN-DCE have lower charging operation time compared to KNN and SVM (58.5 and 52.5 min, column A + C in Table 13). When demand is increased on Day-2 (the number of vehicles is increased to 50%), the proposed CNN-DCE performs best, with the lowest average charging time (53.9 min) compared to the other three methods (57.8 min for ANN, 74.7 min for KNN, and 68.5 min for SVM). The result shows that when charging demand is high, the performance of KNN is decreased due to the imprecise estimation of charger occupancy. It leads to additional queuing delays. It is noticed that CNN-DCE has zero waiting times for the fleet (0.4 h) compared to ANN (15.1 h), KNN (15.4 h), and SVM (14.0 h). Similarly, the performance of the proposed CNN-DCE for the other three days was also the best compared to ANN, KNN, and SVM. The charging operation times could be further decreased by incorporating more fast chargers with the proposed CNN-DCE.

We observe that CNN-DCE and ANN have lower mean passenger waiting time (8.2 min and 9.4 min) and journey time (35.5 min and 38.0 min) for Day-1 with 900 vehicles. The rate of served customers is increased 5% and 3.2% for CNN-DCE and ANN methods. When demand is increased (Day-2 of Table 13), the rate of served customers is increased to 12.4% for CNN-DCE compared to ANN. For all the other days, the proposed CNN-DCE performed the best compared to other methods. We conclude that adopting CNN-DCE significantly reduces vehicle charging times and waiting time for charging for all the test days. In terms of the impact of the proposed CNN-DCE on customer inconvenience, several

Table 13: Performance of the proposed CNN-DCE and the three other methods.

Test days	Number of vehicles	Algorithm	Charging operation per vehicle						Customer inconvenience			
			Average waiting time* A	(SD) B	Average charging time* C	(SD) D	A + C	B + D	Total waiting time of the fleet (hours)	Mean waiting time (m)	Mean journey time (m)	Rate of served customers (%)
Day-1	900	KNN	4.6	14.2	62.5	8.2	67.1	22.4	8.1	10.2	40.3	76.4
		SVM	3.8	12.6	60.3	15.6	64.1	28.2	9.3	12.3	35.1	84.8
		ANN	2.4	13.4	56.1	21.6	58.5	35.0	3.1	9.4	38.0	92.5
		CNN-DCE	0	0	52.5	15.6	52.5	15.6	0	8.2	35.5	96.8
Day-2	1350	KNN	7.5	16.8	74.7	17.2	82.2	34.0	15.4	17.4	34.2	67.4
		SVM	5.2	13.1	68.5	14.5	73.7	37.6	14.0	16.3	30.5	70.4
		ANN	3.8	12.9	57.8	14.2	61.6	37.1	15.1	17.8	41.3	81.6
		CNN-DCE	1.3	8.4	53.9	10.3	55.2	18.7	0.4	14.2	45.5	93.2
Day-3	1100	KNN	6.7	15.2	68.3	12.4	75.0	27.6	9.7	13.6	29.3	70.2
		SVM	4.1	12.9	62.9	15.1	67.0	28.0	9.2	13.2	37.2	71.3
		ANN	3.2	12.3	55.3	13.7	58.5	26.0	8.5	13.0	40.3	82.8
		CNN-DCE	1.1	7.8	51.5	13.3	52.6	21.1	1.2	12.5	37.8	94.3
Day-4	1000	KNN	6.2	14.9	70.2	10.3	76.4	25.2	5.8	11.6	44.2	75.8
		SVM	3.9	12.6	61.2	10.6	65.1	23.2	4.3	11.8	39.0	84.6
		ANN	3.1	12.1	53.4	9.2	56.5	21.3	4.4	11.3	35.4	88.5
		CNN-DCE	1.0	7.2	50.1	8.5	51.1	15.7	0.7	10.3	40.5	96.4
Day-5	1200	KNN	6.9	15.5	69.5	19.2	76.4	34.7	6.3	14.3	39.2	68.4
		SVM	5.6	13.3	63.1	18.5	68.7	31.8	4.2	13.7	44.2	70.8
		ANN	3.6	12.9	56.1	12.4	59.7	25.3	1.1	13.5	40.5	81.6
		CNN-DCE	1.5	9.1	51.8	10.6	53.3	19.7	0.5	12.8	35.8	92.5

Table 14: Waiting time of EVs under different cases.

Cases	Battery capacity (Ah)	Station number	Charger number	Waiting time (minutes)		
				Individual EV	Average	maximum
1	80	4	5	25	22.1	45
2	80	6	10	25.2	22.3	42.5
3	100	12	13	21.4	18.6	43.7
4	80	5	6	25.5	22.2	32.4
5	120	14	2	19.6	16.5	30.2
6	80	2	14	2.8	22.5	42
7	120	7	8	20.4	16	35.8
8	120	9	11	20	16.5	40.5
9	120	10	7	19.8	16.7	35.8

factors might be influenced, such as the configuration of charging infrastructure, driving range of the vehicle, configuration of the fleet, and the spatial distribution of customer demand. The effectiveness of the proposed CNN-DCE is evaluated by conducting further studies based on routing models and different vehicle dispatching with the same demand.

The total queuing time of EVs studied using nine different scenarios and comparison result is shown in Table 14. It is noticed from Table 14 that the average waiting time is mainly influenced by the capacity of the battery packs (refer to cases 1, 2, 4, 5, and 8). In the same way, the waiting time for recharging EVs slightly decreases when the capacity of the battery increases (refer to cases 3, 6, 7, and 9). Although high-capacity batteries reduce the waiting time of EVs, they require more power.

6. Conclusion

In this study, FPOA optimized convolutional neural network-based electric vehicle charging station expansion is proposed. Various hyperparameters of the CNN were optimized using the proposed FPOA algorithm, which delivered optimal solution during training. 20% of the data were randomly selected for testing, and the remaining 80% of data were used for training from the total. The training accuracy of 8.15% was achieved using the optimized CNN compared to the nonoptimized method. The growth of the load is properly analyzed, and the expansion of capacity is planned accordingly. From the results, it is observed that wind energy is expanded more when compared to solar energy since its profile is wider, meaning wind energy expansion is 180% greater

when compared to solar energy. In the overall expansion cost, 53% of the cost is contributed by wind resources and 23% by the microturbine. The operation of energy storage devices and microturbine is optimized, and the microturbine operates at nonpeak loading hours, that is, 17–22 hours. Finally, a numerical analysis has been conducted for five different days to investigate the performance of the proposed method. When demand is increased (around 50%), the rate of served customers for the proposed CNN-DCE is increased to 12.4% compared to ANN.

Data Availability

The data used to support the findings of this study are available from the corresponding author upon request.

Conflicts of Interest

The authors declare no conflicts of interest.

References

[1] Tesla, "Model S," https://www.teslamotors.com/models.

[2] U.S. Department of Energy, "EV everywhere grand challenge road to success," 2014, http://energy.gov.

[3] Y. Fan, S. Yin, S. Zhou, D. Li, C. Fang, and S. Lin, "Electric vehicle charging current scenario generation based on generative adversarial network combined with clustering algorithm," *International Transactions on Electrical Energy Systems*, vol. 31, no. 8, 2021.

[4] Y. Xiong, Bo An, and S. Kraus, "Electric vehicle charging strategy study and the application on charging station placement," *Autonomous Agents and Multi-Agent Systems*, vol. 35, pp. 1–19, 2020.

[5] State Department of Transportation, "Washington state electric vehicle action plan," 2015, http://www.wsdot.wa.gov.

[6] C. Light, "The impact of electric vehicles on system load," 2010, https://www.seattle.gov.

[7] R. V. Krishnakumar, K. R. Vigna, V. Gomathi, J. B. Ekanayake, and S. K. Tiong, "Modelling and simulation of variable speed pico hydel energy storage system for microgrid applications," *Journal of Energy Storage*, vol. 24, pp. 1–14, 2019.

[8] B. Rajani and D. Chandra Sekhar, "A hybrid optimization based energy management between electric vehicle and electricity distribution system," *International Transactions on Electrical Energy Systems*, vol. 31, no. 6, 2021.

[9] S. S. Reddy, V. Sandeep, and C.-M. Jung, "Review of stochastic optimization methods for smart grid," *Frontiers in Energy*, vol. 11, no. 2, pp. 197–209, 2017.

[10] M. I. Alomoush, "Microgrid combined power-heat economic-emission dispatch considering stochastic renewable energy resources, power purchase and emission tax," *Energy Conversion and Management*, vol. 200, pp. 1–20, 2019.

[11] S. S. Reddy and P. R. Bijwe, "Real time economic dispatch considering renewable energy resources," *Renewable Energy*, vol. 83, pp. 1215–1226, 2015.

[12] R. Hemmati, H. Saboori, and P. Siano, "Coordinated short-term scheduling and long-term expansion planning in microgrids incorporating renewable energy resources and energy storage systems," *Energy*, vol. 134, pp. 699–708, 2017.

[13] Q. Tang, M. Xie, K. Yang, Y. Luo, D. Zhou, and Y. Song, "A decision function based smart charging and discharging strategy for electric vehicle in smart grid," *Mobile Networks and Applications*, vol. 24, no. 5, pp. 1722–1731, 2018.

[14] M. A. Hossain, H. R. Pota, S. Squartini, F. Zaman, and K. M. Muttaqi, "Energy management of community microgrids considering degradation cost of battery," *Journal of Energy Storage*, vol. 22, pp. 257–269, 2019.

[15] S. S. Reddy, "Optimal scheduling of thermal-wind-solar power system with storage," *Renewable Energy*, vol. 101, pp. 1357–1368, 2017.

[16] S. S. Reddy, "Optimal power flow with renewable energy resources including storage," *Electrical Engineering*, vol. 99, no. 2, pp. 685–695, 2017.

[17] C. Balasundar, C. K. Sundarabalan, J. Sharma, N. S. Srinath, and J. M. Guerrero, "Design of power quality enhanced sustainable bidirectional electric vehicle charging station in distribution grid," *Sustainable Cities and Society*, vol. 74, p. 103242, 2021.

[18] C. Li, L. Zhang, Z. Ou, Q. Wang, D. Zhou, and J. Ma, "Robust model of electric vehicle charging station location considering renewable energy and storage equipment," *Energy*, vol. 238, p. 121713, 2022.

[19] L. Pan, E. Yao, Y. Yang, and R. Zhang, "A location model for electric vehicle (EV) public charging stations based on drivers' existing activities," *Sustainable Cities and Society*, vol. 59, p. 102192, 2020.

[20] C. Chellaswamy, V. Nagaraju, and R. Muthammal, "Solar and wind energy based charging station for electric vehicles," *International Journal of Advanced Research in Electrical, Electronics and Instrumentation Engineering*, vol. 7, no. 1, pp. 313–324, 2018.

[21] T. D. Chen and K. M. Kockelman, "The electric vehicle charging station location problem: a parking-based assignment method for Seattle," in *Proceedings of the Transportation Research Board 92nd Annual Meeting*, Washington, DC, USA, 2013.

[22] I. Frade, A. Ribeiro, G. Gonçalves, and A. P. Antunes, "Optimal location of charging stations for electric vehicles in a neighborhood in Lisbon, Portugal," *Transportation Research Record: Journal of the Transportation Research Board*, vol. 2252, no. 1, pp. 91–98, 2011.

[23] M. Kuby and S. Lim, "The flow-refueling location problem for alternative-fuel vehicles," *Socio-Economic Planning Sciences*, vol. 39, no. 2, pp. 125–145, 2005.

[24] F. Baouche, R. Billot, R. Trigui, and N.-E. El Faouzi, "Efficient allocation of electric vehicles charging stations: optimization model and application to a dense urban network," *IEEE Intelligent Transportation Systems Magazine*, vol. 6, no. 3, pp. 33–43, 2014.

[25] S. H. Chung and C. Kwon, "Multi-period planning for electric car charging station locations: a case of Korean Expressways," *European Journal of Operational Research*, vol. 242, no. 2, pp. 677–687, 2015.

[26] F. Pan, R. Bent, A. Berscheid, and D. Izraelevitz, "Locating PHEV exchange stations in V2G," in *Proceedings of the First IEEE International Conference on Smart Grid Communications*, pp. 173–178, Gaithersburg, MD, USA, 2010.

[27] A. Ravichandran, S. Sirouspour, P. Malysz, and A. Emadi, "A chance-constraints-based control strategy for microgrids with energy storage and integrated electric vehicles," *IEEE Transactions on Smart Grid*, vol. 99, pp. 1–14, 2016.

[28] X. Xi, R. Sioshansi, and V. Marano, "Simulation-optimization model for location of a public electric vehicle charging infrastructure," *Transportation Research Part D: Transport and Environment*, vol. 22, pp. 60–69, 2013.

[29] H.-Y. Mak, Y. Rong, and Z.-J. M. Shen, "Infrastructure planning for electric vehicles with battery swapping," *Management Science*, vol. 59, no. 7, pp. 1557–1575, 2013.

[30] S. Surender Reddy and P. R. Bijwe, "Day-ahead and real time optimal power flow considering renewable energy resources," *International Journal of Electrical Power & Energy Systems*, vol. 82, pp. 400–408, 2016.

[31] H. Mehrjerdi and R. Hemmati, "Stochastic model for electric vehicle charging station integrated with wind energy," *Sustainable Energy Technologies and Assessments*, vol. 37, pp. 1–6, Article ID 100577, 2020.

[32] Z. Zhu, S. Lambotharan, W. H. Chin, and Z. Fan, "A stochastic optimization approach to aggregated electric vehicles charging in smart grids," in *Proceedings of the 2014 IEEE Innovative Smart Grid Technologies - Asia*, pp. 51–56, ISGT ASIA, Kuala Lumpur, Malaysia, 2014.

[33] R. S. Sutton and A. Barto, *Reinforcement Learning: An Introduction*, MIT Press, Cambridge, MA, USA, 2nd edition, 2018.

[34] O. I. Abiodun, A. Jantan, A. E. Omolara, K. V. Dada, N. A. Mohamed, and H. Arshad, "State-of-the-art in artificial neural network applications: a survey," *Heliyon*, vol. 4, no. 11, Article ID e00938, 2018.

[35] M. A. Masmoudi, M. Hosny, E. Demir, K. N. Genikomsakis, and N. Cheikhrouhou, "The dial-a-ride problem with electric vehicles and battery swapping stations," *Transportation Research Part E: Logistics and Transportation Review*, vol. 118, pp. 392–420, 2018.

[36] W. Jie, J. Yang, M. Zhang, and Y. Huang, "The two-echelon capacitated electric vehicle routing problem with battery swapping stations: formulation and efficient methodology," *European Journal of Operational Research*, vol. 272, no. 3, pp. 879–904, 2019.

[37] C. Li, T. Ding, X. Liu, and C. Huang, "An electric vehicle routing optimization model with hybrid plug-in and wireless charging systems," *IEEE Access*, vol. 6, pp. 27569–27578, 2018.

[38] A. Froger, J. E. Mendoza, O. Jabali, and G. Laporte, "Improved formulations and algorithmic components for the electric vehicle routing problem with nonlinear charging functions," *Computers & Operations Research*, vol. 104, pp. 256–294, 2019.

[39] M. Bruglieri, S. Mancini, and O. Pisacane, "Solving the green vehicle routing problem with capacitated alternative fuel stations," in *Proceedings of the 16th Cologne-Twente Workshop on Graphs and Combinatorial Optimization*, pp. 196–199, Paris, France, 2018.

[40] G. Aghajani and N. Yousefi, "Multi-objective optimal operation in a micro-grid considering economic and environmental goals," *Evolving Systems*, vol. 10, no. 2, pp. 239–248, 2019.

[41] X.-S. Yang, *Flower Pollination Algorithm for Global Optimization*, UCNC. Springer, Berlin, Germany, 2012.

[42] Y. Zhou, S. Zhang, Q. Luo, and C. Wen, "Using flower pollination algorithm and atomic potential function for shape matching," *Neural Computing & Applications*, vol. 29, no. 6, pp. 21–40, 2018.

[43] P. Ong, D. D. V. S. Chin, C. S. Ho, and C. H. Ng, "Modeling and optimization of cold extrusion process by using response surface methodology and metaheuristic approaches," *Neural Computing & Applications*, vol. 29, no. 11, pp. 1077–1087, 2018.

[44] Z. A. A. Alyasseri, M. AzmiAl-Betar, M. A. Awadallah et al., "A hybrid flower pollination with β-hill climbing algorithm for global optimization," *Journal of King Saud University - Computer and Information Sciences*, 2021, In press.

[45] M. A. M. Ramli, H. R. E. H. Bouchekara, and A. S. Alghamdi, "Optimal sizing of PV/wind/diesel hybrid microgrid system using multi-objective self-adaptive differential evolution algorithm," *Renewable Energy*, vol. 121, pp. 400–411, 2018.

[46] C. H. Dharmakeerthi, N. Mithulananthan, and T. K. Saha, "A comprehensive planning framework for electric vehicle charging infrastructure deployment in the power grid with enhanced voltage stability," *International Transactions on Electrical Energy Systems*, vol. 25, no. 6, pp. 1–19, 2014.

[47] E. Samadi, B. Ali, and R. Ebrahimpour, "Decentralized multiagent based energy management of microgrid using reinforcement learning," *International Journal of Electrical Power & Energy Systems*, vol. 122, pp. 1–13, 2020.

[48] H. Mehrjerdi and E. Rakhshani, "Optimal operation of hybrid electrical and thermal energy storage systems under uncertain loading condition," *Applied Thermal Engineering*, vol. 160, pp. 1–6, 2019.

[49] C. Chellaswamy, L. Balaji, and T. Kaliraja, "Renewable energy based automatic recharging mechanism for full electric vehicle," *Engineering Science and Technology, an International Journal*, vol. 23, no. 3, pp. 555–564, 2020.

[50] M. Zukerman, "Introduction to queueing theory and stochastic teletraffic models," 2013, https://arxiv.org/abs/1307.2968.

[51] J. Asamer, M. Reinthaler, M. Ruthmair, M. Straub, and J. Puchinger, "Optimizing charging station locations for urban taxi providers," *Transportation Research Part A: Policy and Practice*, vol. 85, pp. 233–246, 2016.

[52] Kaggle, "Datasets," https://www.kaggle.com.

[53] Data World, "Datasets," https://data.world/datasets.